

Uncertainties in MEPS@NLO calculations of $h + \text{jets}$ Stefan Höche,^{1,*} Frank Krauss,^{2,†} and Marek Schönherr^{2,‡}¹*SLAC National Accelerator Laboratory, Menlo Park, California 94025, USA*²*Institute for Particle Physics Phenomenology, Durham University, Durham DH1 3LE, United Kingdom*

(Received 30 January 2014; published 8 July 2014)

Uncertainties in the simulation of Higgs boson production with up to two jets at next-to-leading-order accuracy are investigated. Traditional uncertainty estimates based on scale variations are extended employing different functional forms for the central scale, and the impact of details in the implementation of the parton shower is discussed.

DOI: 10.1103/PhysRevD.90.014012

PACS numbers: 12.38.Bx, 13.85.-t, 13.87.-a

I. INTRODUCTION

After the discovery of a Standard Model–like Higgs boson at run I of the LHC operations [17] further studies of the properties of the new particle will become a focal point of the physics programme during run II. Anticipating the effect of the scheduled significantly larger collision energy of the protons translating into increased energies available for colliding partons, and a vastly increased luminosity, more production and decay channels and combinations of both become available for studying the coupling of the Higgs boson to other particles. In particular, production channels such as the production of the Higgs boson in weak boson fusion, yielding two additional jets, or its production in the boosted regime will provide challenging tests for the Brout-Englert-Higgs mechanism of mass generation [18].

With increasing accuracy in experimental measurements, theoretical computations are inevitably required to become more precise. For the dominant production of the Higgs boson through gluon-induced heavy quark loops, tremendous progress has been made over the past years to achieve the necessary precision, for example with calculations at the next-to-next-to-leading-order accuracy (NNLO) in the perturbative expansion of the strong coupling: In the past year the by now routinely employed result for $pp \rightarrow h$ through gluon fusion in the effective theory [19] (for $m_t \ll m_h$) has been supplemented with a calculation for $pp \rightarrow h + \text{jet}$ [20] in the all-gluon channel. Mass effects in the heavy quark loop, going beyond the usual effective theory approach, were evaluated in [21]. Even a complete N³LO calculation of $pp \rightarrow h$ is being finalized at the moment, with first results already reported [22]. Mixed QCD and electroweak two-loop corrections have been evaluated in an effective theory approach [23] and assuming complete factorization [24]. At NLO accuracy, due to the level of automation achieved by now, the production of the Higgs boson in association with two [25] and three jets

[26] through the effective vertex has been investigated. Due to the gluon initial states, resummation plays an important role at small transverse momenta of the Higgs boson, and whenever two jets are separated by a large transverse momentum or angular distance. Results for the transverse momentum in inclusive production at NNLO + NNLL accuracy, are available for example in [27]. Jet vetoes, which are particularly relevant for the Higgs boson decaying into W bosons have been discussed in [28].

Parton-shower based simulations, typically used by the experiments, usually lag behind analytical calculations by at least one perturbative order. This is exemplified by the highest accuracy in simulating this process so far, which achieves the NNLO level through a suitable reweighting in the MinLO procedure [29]. At the next-to-leading-order accuracy, parton-shower matched calculations have been provided using the POWHEG [14] and MC@NLO [3] methods. Recently, the MC@NLO algorithm has been modified in order to include color-suppressed but logarithmically enhanced contributions in the first emission term of the parton shower, and in the corresponding Sudakov factor [1,30]. This method, which we call S-MC@NLO also forms the basis of a multijet merging algorithm based on NLO calculations [2]. This merging method is similar in spirit to the by now traditional multijet merging for LO matrix elements [15,16,31,32]. The new NLO algorithm was successfully applied to a number of relevant physics cases, most notably to jet vetoes in W -pair backgrounds to Higgs boson production at the LHC [33] and to top-quark pair production and the asymmetries encountered at the Tevatron [34]. A closely related multijet merging algorithm has also been proposed in [10,35], while [11] relies on ideas in line with the MLM multijet merging prescription for leading order calculations [36]. Matching methods like POWHEG can be extended with appropriate scale choices and Sudakov suppression factors, which allows to extrapolate the matched NLO calculation for $X + \text{jet}$ production to the zero- p_T region, thus leading to NLO accurate results also for X production, where X is a colorless final state. This has been dubbed the MinLO technique [12,13]. In contrast to the genuine merging methods listed

*shoeche@slac.stanford.edu

†frank.krauss@durham.ac.uk

‡marek.schoenherr@durham.ac.uk

TABLE I. Evolution parameters for the parton shower. We use the variables defined in [5].

Scheme	Final state	Initial state
0	$2p_i p_j \tilde{z}_{i,jk} (1 - \tilde{z}_{i,jk})$	$2p_a p_j (1 - z_{a,jk})$
1	$2p_i p_j \begin{cases} \tilde{z}_{i,jk} (1 - \tilde{z}_{i,jk}) & \text{if } i, j = g \\ 1 - \tilde{z}_{i,jk} & \text{if } j = g \\ \tilde{z}_{i,jk} & \text{if } i = g \\ 1 & \text{else} \end{cases}$	$2p_a p_j \begin{cases} 1 - z_{a,jk} & \text{if } j = g \\ 1 & \text{else} \end{cases}$

above, this scheme has not yet been extended to higher-multiplicity processes.

For the sub-dominant production of a Higgs boson through weak vector boson fusion (VBF) [37], which becomes a very interesting channel when jet vetoes between the two relatively forward tagging jets are applied [38], NLO QCD corrections in the structure function approach assume a relatively simple form. They have been known for a long time [39]. NNLO corrections in this approach have more recently been computed in [40], while QCD NLO corrections for $pp \rightarrow h + 3$ jet production in VBF were discussed in [41]. The electroweak NLO corrections to VBF Higgs boson production [42] were found to be of roughly the same size as the QCD ones. On the level of parton–shower based simulations, this topology is available through both the POWHEG and the MC@NLO algorithms [43].

In this paper, a next-to-leading order plus parton shower merged calculation is presented for the production of a Higgs boson through gluon fusion in the effective theory approximation with up to two additional jets at NLO and a third jet at LO accuracy. For these studies the Monte Carlo event generator SHERPA [44] is used in conjunction with virtual corrections taken from MCFM [25,45]. The focus of the study rests on the accurate description both of the rate and of those kinematical distributions of the various objects in the final state, which are central to analyses involving typical VBF cuts. The fully exclusive nature of a Monte Carlo simulation using a general-purpose event generator ensures, however, that a wide range of inclusive and exclusive observables can be analyzed simultaneously. The most relevant uncertainties in the simulation are detailed and some substantial differences between one-jet and two-jet NLO-merged simulations are pointed out. Special attention is paid to uncertainties related to the functional form of scale in the fixed-order NLO calculation, which massively exceed those obtained from a mere variation of a constant scale factor in the conventional range from 1/2 to 2.

This manuscript is organized as follows: Section II reviews the methods used in the simulation, with emphasis on the actual multijet merging algorithm. Section III presents predictions obtained with the event generator SHERPA and discusses related uncertainties. An outlook is given in Sec. IV.

II. METHODS

This section briefly summarizes the S–MC@NLO matching method and the MEPS@NLO merging technique. We emphasize only those aspects of the implementation in SHERPA which are relevant to the assessment of uncertainties of the simulation. Details of the two algorithms are described in [1] and [2].

A. Matrix-element parton-shower matching

The action of the parton shower on an arbitrary parton-level final state can be expressed in terms of a generating functional, $\mathcal{F}_n(t)$, where n is the number of existing partons, and t is the parton shower starting scale. The value of an infrared safe observable, O , in the Born approximation is then computed as

$$\langle O \rangle^{(\text{PS})} = \int d\Phi_B \mathbf{B}(\Phi_B) \mathcal{F}_0(\mu_F^2, O), \quad (1)$$

with $d\Phi_B$ the differential Born phase space element and $\mathbf{B}(\Phi_B)$ the Born differential cross section. The generating functional of the parton shower reads

$$\mathcal{F}_n(t, O) = \Delta_n(t_c, t) O(\Phi_n) + \int_{t_c}^t d\Phi'_1 \mathbf{K}_n(\Phi'_1) \Delta_n(t', t) \mathcal{F}_{n+1}(t', O) \quad (2)$$

with $\mathbf{K}_n(\Phi_1)$ the parton shower splitting kernel on the n parton state and $\Delta_n(t', t)$ is the corresponding Sudakov form factor. The single parton emission phase space is parametrized as $d\Phi_1 = dt dz d\phi J(t, z, \phi)$. In this context $t \equiv t(\Phi_1)$ is the evolution variable, z is the splitting variable, ϕ is the azimuthal angle of the splitting and $J(t, z, \phi)$ is the associated Jacobian. t_c is the infrared cutoff. While the first term in Eq. (2) describes the no-emission probability, the second term describes a single independent emission at scale t' including the ensuing iteration with the boundary conditions of the newly formed state.

The MC@NLO matching method promotes Eq. (1) to NLO accuracy using a modified subtraction scheme [3]. This technique was extended in [1] such that the first emission in the shower is generated in a fully coherent manner, and therefore all singularities of the real-emission matrix element are properly subtracted. This applies in

TABLE II. Mapping of variables for parton shower kinematics in scheme 0 [see Eqs. (6) and (7)].

Configuration	$z_{i,jk}$	$y_{ij,k}$	Configuration	$z_{j,ak}$	$y_{aj,k}$
Final-Final	$\frac{p_i p_k}{(p_i + p_j) p_k}$	$\frac{p_i p_j}{p_i p_j + (p_i + p_j) p_k}$	Initial-Final	$\frac{p_j p_k}{(p_a - p_j) p_k}$	$\frac{p_a p_j}{p_a p_j + (p_a - p_j) p_k}$
Final-Initial	$\frac{p_i p_k}{(p_i + p_j) p_k}$	$\frac{p_i p_j}{p_i p_j - (p_i + p_j) p_k}$	Initial-Initial	$\frac{p_j p_k}{(p_a - p_j) p_k}$	$\frac{p_a p_j}{p_a p_j - (p_a - p_j) p_k}$

particular to terms which are suppressed by $1/N_c$. We will refer to the latter method as S–MC@NLO.

In S–MC@NLO, any observable O is computed as

$$\langle O \rangle^{(S\text{-MC@NLO})} = \int d\Phi_B \bar{\mathbf{B}}^{(A)}(\Phi_B) \mathcal{F}^{(A)}(\mu_Q^2, O) + \int d\Phi_R \mathbf{H}^{(A)}(\Phi_R) \mathcal{F}_1(t, O), \quad (3)$$

where $\bar{\mathbf{B}}^{(A)}$ and $\mathbf{H}^{(A)}$ are the next-to-leading-order weighted differential cross section and the hard remainder function, given by

$$\begin{aligned} \bar{\mathbf{B}}^{(A)}(\Phi_B) &= \mathbf{B}(\Phi_B) + \tilde{\mathbf{V}}(\Phi_B) + \mathbf{I}^{(S)}(\Phi_B) \\ &+ \int d\Phi_1 [\mathbf{D}^{(A)}(\Phi_B, \Phi_1) \Theta(\mu_Q^2 - t) \\ &- \mathbf{D}^{(S)}(\Phi_B, \Phi_1)], \\ \mathbf{H}^{(A)}(\Phi_R) &= \mathbf{R}(\Phi_R) - \mathbf{D}^{(A)}(\Phi_R) \Theta(\mu_Q^2 - t). \end{aligned} \quad (4)$$

Here we have introduced the virtual corrections, $\tilde{\mathbf{V}}(\Phi_B)$, the real-emission corrections, $\mathbf{R}(\Phi_R)$, and the corresponding real-emission phase space element, $d\Phi_R$. Most importantly, the dipole subtraction terms are given by $\mathbf{D}(\Phi_B, \Phi_1)$ in unintegrated form, and by $\mathbf{I}(\Phi_B)$ in integrated form. We distinguish between fixed-order subtraction terms, $\mathbf{D}^{(S)}$ and shower subtraction terms, $\mathbf{D}^{(A)}$. Both must have the same kinematics mapping, however their functional form away from the singular limits of the real emission corrections may differ. In particular, we implement an upper cutoff in the parton-shower evolution parameter in $\mathbf{D}^{(A)}$ only, which is referred to as the resummation scale μ_Q .

The differential real-emission phase space element factorizes as $d\Phi_R = d\Phi_B d\Phi_1$ with the above parametrization for $d\Phi_1$. This factorization allows to define a generating functional $\mathcal{F}^{(A)}(t, O)$ of the S–MC@NLO as

$$\begin{aligned} \mathcal{F}^{(A)}(t, O) &= \Delta^{(A)}(t_c, t) O(\Phi_B) + \int_{t_c}^t d\Phi_1' \frac{\mathbf{D}^{(A)}(\Phi_B, \Phi_1')}{\mathbf{B}(\Phi_B)} \\ &\times \Delta^{(A)}(t', t) \mathcal{F}_1(t', O) \end{aligned} \quad (5)$$

with $\Delta^{(A)}(t_c, t)$ the Sudakov factor of the S–MC@NLO, and $\mathbf{D}^{(A)}(\Phi_B, \Phi_1')/\mathbf{B}(\Phi_B)$ its splitting kernels. Again, the first term in Eq. (5) is simply a no-emission probability, while the second term now describes one fully coherent emission from the S–MC@NLO. Any further radiation is

implemented in the parton-shower approximation, as indicated by $\mathcal{F}_1(t', O)$.

We employ a parton shower based on Catani-Seymour dipole subtraction [4]. To assess the uncertainty arising from the choice of evolution variable, we implement two different options, which are listed in Table I. Their impact on experimental observables is analyzed in Sec. III. The reasoning behind scheme 1 is that for splittings without soft gluon enhancement, there is no z or $1 - z$ pole in the splitting function. Ordering the splittings in transverse momentum, as done in scheme 0, might thus be inappropriate.

In addition, two different kinematics mappings are implemented, which were described and compared in detail in [6]. We denote the original mapping, proposed in [4] and derived from [5] by ‘‘scheme 1’’, while the second mapping is denoted as ‘‘scheme 0’’. This scheme can be described as follows [6]¹:

Particle momenta after the splitting process $\tilde{ij} \rightarrow ij$ in the presence of a spectator k are expressed in terms of the original momenta, \tilde{p}_{ij} and \tilde{p}_k , as²

$$\begin{aligned} p_i^\mu &= z_{i,jk} \tilde{p}_{ij}^\mu + \frac{k_\perp^2}{z_{i,jk}} \frac{\tilde{p}_k^\mu}{2\tilde{p}_{ij}\tilde{p}_k} + k_\perp^\mu, \\ p_j^\mu &= (1 - z_{i,jk}) \tilde{p}_{ij}^\mu + \frac{k_\perp^2}{1 - z_{i,jk}} \frac{\tilde{p}_k^\mu}{2\tilde{p}_{ij}\tilde{p}_k} - k_\perp^\mu, \end{aligned} \quad (6)$$

where

$$k_\perp^2 = 2\tilde{p}_{ij}\tilde{p}_k y_{ij,k} z_{i,jk} (1 - z_{i,jk}). \quad (7)$$

The parameters $z_{i,jk}$ and $y_{ij,k}$ depend on the type of splitting and are given for all dipole configurations in Table II. The spectator momentum p_k is determined by momentum conservation. In the case of initial state splitter or spectator partons, a proper Lorentz transformation is applied to keep both initial state particles aligned along the beam axis.

In scheme 1, initial-state splittings with final state spectator are instead constructed as if they were final-state splittings with initial state spectator, by replacing $\tilde{z}_j \rightarrow u_j$, $p_k \rightarrow -p_i$ and $p_j \rightarrow p_k$.

Schematically the two mapping schemes differ in how the recoil is distributed in initial state splittings with final

¹A similar scheme for dipole showers has also been discussed in [7].

²We work in the five-flavor scheme and therefore consider massless partons only. All momenta are taken as outgoing.

state spectator. In scheme 0 the entire final state recoils, while in scheme 1 only the spectator parton recoils. The two schemes are linked by a proper Lorentz transformation, which was worked out in [7].

B. Multijet merging

The S–MC@NLO method augments NLO fixed-order calculations with the simple resummation encoded in the parton shower. Compared to pure fixed-order calculations, this allows more meaningful definitions of jet cross sections, because logarithms of the jet transverse momentum cutoff are resummed to (at least) leading logarithmic accuracy. The precision of such a simulation can be extended further by correcting emissions from the parton shower with fixed-order results for higher jet multiplicity. This has been achieved in a genuine form both at leading order [8,9] and at next-to-leading order [2,10,11]. The MiNLO method can be used to the same ends, albeit only for zero and one additional jet [12,13]. While the merging at LO is straightforward, it requires

additional care at NLO to properly subtract the first-order expansion of the shower expression. This procedure is vital to preserve the logarithmic accuracy of the parton shower [2,10].

It is instructive to analyze the contribution to an observable O from the exclusive simulation of final states with n hard partons. Additional partons may be present, which are not resolved according to a technical jet cut, Q_{cut} , called the merging cut. The observable Q in which the merging cut is specified is called the merging criterion. It may or may not be identical to an experimental jet definition, however, to make the calculation useful in practice, one should choose the two variables as similar as possible. In addition, Q_{cut} should be chosen such that the entire phase space probed by a measurement is covered by the appropriate NLO calculation. In practice this means that Q_{cut} should effectively fall below the experimental jet cut.

The exclusive contribution to the observable with exactly n hard partons reads

$$\begin{aligned} \langle O \rangle_n^{\text{excl}} = & \int d\Phi_n \Theta(Q(\Phi_n) - Q_{\text{cut}}) \tilde{\text{B}}_n^{(\text{A})}(\Phi_n) \tilde{\mathcal{F}}_n^{(\text{A})}(\mu_Q^2, O; < Q_{\text{cut}}) \\ & + \int d\Phi_{n+1} \Theta(Q(\Phi_n) - Q_{\text{cut}}) \Theta(Q_{\text{cut}} - Q(\Phi_{n+1})) \tilde{\text{H}}_n^{(\text{A})}(\Phi_{n+1}) \tilde{\mathcal{F}}_{n+1}^{(\text{A})}(\mu_Q^2, O; < Q_{\text{cut}}). \end{aligned} \quad (8)$$

In this context, we have introduced a new generating functional, $\tilde{\mathcal{F}}_n(\mu_Q^2, O; < Q_{\text{cut}})$, which represents a truncated vetoed parton shower [14,15]. It implements emissions on a parton shower tree that corresponds to the n -parton final state. It also computes the survival probability for that particular configuration, indicated by the notation $< Q_{\text{cut}}$. The starting conditions must be chosen carefully in order not to spoil the accuracy of the calculation: Each possible shower topology is selected according to the exact forward branching probability of the shower into the given configuration. This scheme was described in great detail in [10,15,16].

The seed cross sections $\tilde{\text{B}}^{(\text{A})}$ and $\text{H}^{(\text{A})}$ as defined in Eq. (4) are replaced by the functions

$$\begin{aligned} \tilde{\text{B}}_n^{(\text{A})}(\Phi_n) = & \text{B}_n(\Phi_n) + \tilde{\text{V}}_n(\Phi_n) + \text{I}_n^{(\text{S})}(\Phi_n) \\ & + \int d\Phi_1 [\tilde{\text{d}}_n^{(\text{A})}(\Phi_n, \Phi_1) - \text{d}_n^{(\text{S})}(\Phi_n, \Phi_1)] \\ \tilde{\text{H}}_n^{(\text{A})}(\Phi_{n+1}) = & \text{R}_n(\Phi_{n+1}) - \tilde{\text{D}}_n^{(\text{A})}(\Phi_{n+1}), \end{aligned} \quad (9)$$

which take the probability of truncated parton shower emissions into account [2]. To this end, the dipole terms used in the S–MC@NLO are extended by the parton-shower emission probabilities, $\text{B}_n(\Phi_n) \text{K}_i(\Phi_{1,n+1})$, where $\text{K}_i(\Phi_{1,n+1})$ is the sum of all shower splitting functions

for the intermediate state with $i < n$ in the predefined shower tree,

$$\begin{aligned} \tilde{\text{D}}_n^{(\text{A})}(\Phi_{n+1}) = & \text{D}_n^{(\text{A})}(\Phi_{n+1}) \Theta(t_n - t_{n+1}) \\ & + \sum_{i=0}^{n-1} \text{B}_n(\Phi_n) \text{K}_i(\Phi_{1,n+1}) \Theta(t_i - t_{n+1}) \\ & \Theta(t_{n+1} - t_{i+1})|_{t_0=\mu_Q^2}. \end{aligned} \quad (10)$$

While seemingly quite complex, Eq. (10) has a very simple physical interpretation: The first term corresponds to the coherent emission of a parton from the external n -parton final state. It contains all soft and collinear singularities which are present in the real-emission matrix elements. The sum in the second term corresponds to emissions from the intermediate states with i partons. They can be implemented in the parton shower approximation, because soft divergences are regulated by the finite mass of the intermediate particles.

In practice the second term in Eq. (10) can be implemented in an NLO-vetoed truncated shower [2]. This is a straightforward modification of an existing shower algorithm. It is far more complicated to select the correct renormalization scale. Two different methods have been proposed to this end, which are both constructed such that

the logarithmic accuracy of the shower is maintained. Their results therefore differ only beyond NLO.

(i) The UNLOPS scale [10]

An arbitrary scale is chosen for the fixed-order NLO calculation. Renormalization terms and collinear mass factorization counterterms are added to restore the scale choice of the parton shower at NLO accuracy. The procedure recovers all logarithms formally resummed by the parton shower, but it does not reproduce its full logarithmic structure as the two-loop running of the strong coupling generates additional terms.

(ii) The CKKW scale [2]

The scale in the fixed-order calculation is chosen such that the coupling factors of the parton shower for the chosen shower history are recovered entirely. Renormalization terms are then exactly zero and only collinear mass factorization counterterms must be added.

We will compare the effects of these two choices in Sec. III, with some different parametrization used for the UNLOPS scale.

III. RESULTS

This section presents results obtained with the MEPS@NLO algorithm applied to Higgs boson production through gluon fusion in association with jets at a center-of-mass energy of 8 TeV. We work in the five flavor scheme. The loop-mediated coupling of the Higgs boson to gluons is calculated in Higgs effective theory (HEFT) [46] with $m_t \rightarrow \infty$. The Born- and real-emission matrix elements as well as the dipole subtraction terms [5] are computed using AMEGIC++ [47]. One-loop matrix elements are implemented according to [48] in the case of $pp \rightarrow h$ and [49] in the case of $pp \rightarrow h + \text{jet}$, or obtained through an interface to MCFM [25,45] in the case of $pp \rightarrow h + 2$ jets. Our calculation is purely perturbative; i.e. hadronization and underlying event contributions are not included. The CT10nlo [50] parton distribution functions are used.

The Higgs boson mass is set to $m_h = 125$ GeV. As we are interested in the properties of the QCD activity accompanying the production of the Higgs boson, no restrictions on its decay are applied. Jets are defined using the anti- k_\perp jet algorithm [51] with $R = 0.4$ and $p_\perp^{\min} = 30$ GeV. Jets are required to have a rapidity of $|y| < 5$. A VBF selection is defined by requiring at least two jets and imposing two additional cuts on the two leading- p_T ones: $|\Delta y_{j_1, j_2}| > 2.8$ and $m_{j_1, j_2} > 400$ GeV, and, where indicated, veto the emission of a third jet inbetween the two leading jets.

Uncertainties of the perturbative calculation arise from a variation of all unphysical scales in the process. While the factorization and renormalization scales, μ_F and μ_R are varied independently within the conventional factor of two, the resummation scale μ_Q is varied by a factor of

$\sqrt{2}$. The merging scale Q_{cut} , separating $pp \rightarrow h + n$ jet from $pp \rightarrow h + (n + 1)$ jet calculations, is varied in the set $\{15, 20, 30\}$ GeV.³ The central scale choices are $\mu_R = \mu_{\text{CKKW}} = \alpha_s^2(m_h)\alpha_s(t_1) \cdots \alpha_s(t_n)$, and $\mu_F = \mu_Q = m_h$. To assess the large relative $\mathcal{O}(\alpha_s^2)$ effects in this process, which arise from the Higgs effective coupling to gluons, two additional functional forms of the renormalization scale are investigated using the UNLOPS method: $\mu_R = m_h$ and $\mu_R = \hat{H}'_T = \sum m_\perp$ (sum of all transverse masses in the final state) [52]. The logarithmic accuracy of the parton shower is preserved in this case by including the renormalization term [2]

$$B_n \frac{\alpha_s(\mu_R)}{\pi} \beta_0 \left(\log \frac{\mu_R}{\mu_{\text{CKKW}}} \right)^{2+n} \quad (11)$$

This term reverts any scale choice to that of μ_{CKKW} to one-loop order, cf. Sec. II. We will choose the prediction for $\mu_R = m_h$ as a reference for comparisons. The CKKW scale and \hat{H}'_T can be regarded as two extreme choices on opposite sides of m_h . While \hat{H}'_T increases in the presence of an additional low- p_T jet, the CKKW scale decreases.

All analyses and plots in this section were made with the help of RIVET [53].

A. Inclusive observables

First we examine inclusive and exclusive (jet) cross sections generated in our simulations. They are summarized in Table III. Although the expressions for the respective quantities are all calculated at next-to-leading-order accuracy and only differ by terms of $\mathcal{O}(\alpha_s^2)$, induced through the different scales used for the strong coupling, the deviations from one another are rather large already. This hints at the well known fact of the poor convergence of the perturbative series in this process. Generally, the computed cross sections are largest with $\mu_R = \mu_{\text{CKKW}}$ and smallest with $\mu_R = \hat{H}'_T$, increasingly so as the hardness of the event increases as required by the respective selection criteria. The inclusive cross section, which is expected to be less sensitive to such kinematic effects, is in good agreement between the different scale choices.

The uncertainties quoted stem from a variation of μ_F and μ_R , μ_Q , and Q_{cut} , varied separately as detailed above and then summed in quadrature. Again, the different choices for the central scale lead to increasingly deviating uncertainty estimates, smallest for $\mu_R = \hat{H}'_T$ and largest for

³The merging scale should not be set to a value above the minimum transverse momentum of the analysis jet definition in order not to degrade the accuracy of the perturbative description of observables involving at least one jet. This avoids muddying the merging scale systematics with leading order vs next-to-leading-order effects.

TABLE III. Cross sections with three different central scales. Uncertainties are given as super- and subscripts and detail, in that order, $\mu_{R/F}$ variations, μ_Q variations, and Q_{cut} variations.

	$\mu_R = \mu_{\text{CKKW}}$	$\mu_R = m_h$	$\mu_R = \hat{H}_T^l$
$\sigma_{0\text{jet}}^{\text{incl}}$	$12.2^{+1.5+0.5+0.2}_{-1.3-0.5-0.2}$ pb	$11.6^{+1.5+0.6+0.3}_{-1.2-0.5-0.2}$ pb	$10.9^{+0.9+0.7+0.3}_{-0.9-0.6-0.2}$ pb
$\sigma_{0\text{jet}}^{\text{excl}}$	$8.05^{+0.65+0.48+0.14}_{-0.66-0.39-0.29}$ pb	$7.71^{+0.73+0.53+0.31}_{-0.70-0.33-0.36}$ pb	$7.37^{+0.60+0.53+0.31}_{-0.59-0.33-0.35}$ pb
$\sigma_{1\text{jet}}^{\text{incl}}$	$4.16^{+0.81+0.10+0.40}_{-0.46-0.31-0.46}$ pb	$3.91^{+0.53+0.28+0.50}_{-0.35-0.18-0.35}$ pb	$3.54^{+0.26+0.29+0.67}_{-0.24-0.18-0.37}$ pb
$\sigma_{1\text{jet}}^{\text{excl}}$	$3.08^{+0.36+0.11+0.29}_{-0.32-0.18-0.30}$ pb	$2.92^{+0.29+0.21+0.30}_{-0.26-0.13-0.30}$ pb	$2.68^{+0.22+0.22+0.30}_{-0.21-0.13-0.30}$ pb
$\sigma_{2\text{jet}}^{\text{incl}}$	$1.07^{+0.46+0.05+0.09}_{-0.15-0.13-0.11}$ pb	$0.99^{+0.24+0.07+0.16}_{-0.09-0.05-0.08}$ pb	$0.86^{+0.04+0.07+0.16}_{-0.04-0.05-0.07}$ pb
$\sigma_{\text{VBF cuts}}^{\text{central jet veto}}$	$0.165^{+0.070+0.005+0.008}_{-0.030-0.022-0.012}$ pb	$0.152^{+0.039+0.007+0.016}_{-0.019-0.007-0.007}$ pb	$0.126^{+0.010+0.007+0.016}_{-0.010-0.007-0.007}$ pb
$\sigma_{\text{VBF cuts}}^{\text{VBF cuts}}$	$0.124^{+0.047+0.002+0.010}_{-0.023-0.015-0.008}$ pb	$0.113^{+0.026+0.007+0.015}_{-0.013-0.006-0.008}$ pb	$0.096^{+0.008+0.007+0.015}_{-0.008-0.006-0.008}$ pb

$\mu_R = \mu_{\text{CKKW}}$. Once cuts are imposed the variation of the unphysical merging scale, Q_{cut} is comparable or even exceeds the scale variation from fixed-order calculations when scale definitions sufficiently different from μ_{CKKW} in the respective regimes are used.

Next we analyze differential distributions. In Fig. 1 and following the lower pane shows the ratio of all simulations with respect to the result from $\mu_R = m_h$. The coarse dashed line shows the contribution to the $\mu_R = m_h$ result from the exclusive NLO calculation for $pp \rightarrow h + 0$ jets, and the fine dashed and dash-dotted lines show the contribution from the exclusive calculations for $pp \rightarrow h + 1$ jet and $pp \rightarrow h + 2$ jets, respectively. The dotted line shows the contribution from the LO result for $pp \rightarrow h + 3$ jets. Uncertainty bands are computed as the quadratic sum of

the renormalization/factorization scale uncertainty in the perturbative calculation, the resummation scale uncertainty and the multijet merging scale uncertainty. Intrinsic parton shower uncertainties will be discussed in detail in Sec. III C.

The transverse momentum distribution of the Higgs boson, and its rapidity spectrum are shown in Fig. 1. Since both are rather inclusive observables, we observe a good agreement of the predictions obtained with different scale choices. The CKKW scale produces a larger uncertainty band than the two others, because at small $p_{T,h}$ it is driven by the transverse momentum of the first jet. This leads to an increase in the inclusive cross section, while the rapidity distribution of the Higgs boson is largely unaffected.

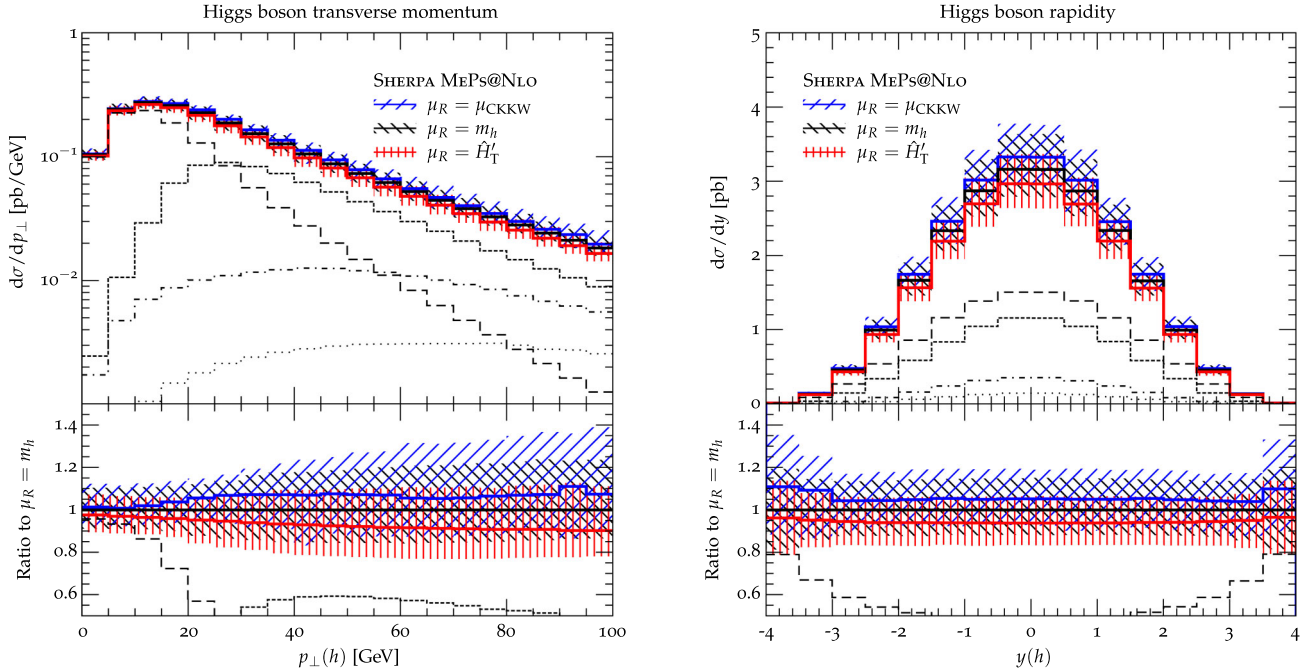


FIG. 1 (color online). Transverse momentum (left) and rapidity (right) of the Higgs boson with three different scale choices. The uncertainty bands include all sources of perturbative uncertainties as a quadratic sum. Coarse dashed lines correspond to the contribution from exclusive 0-jet hard scattering configurations, fine dashed lines to exclusive 1-jet configurations, dash-dotted lines to exclusive 2-jet configurations and dotted lines to inclusive 3-jet configurations.

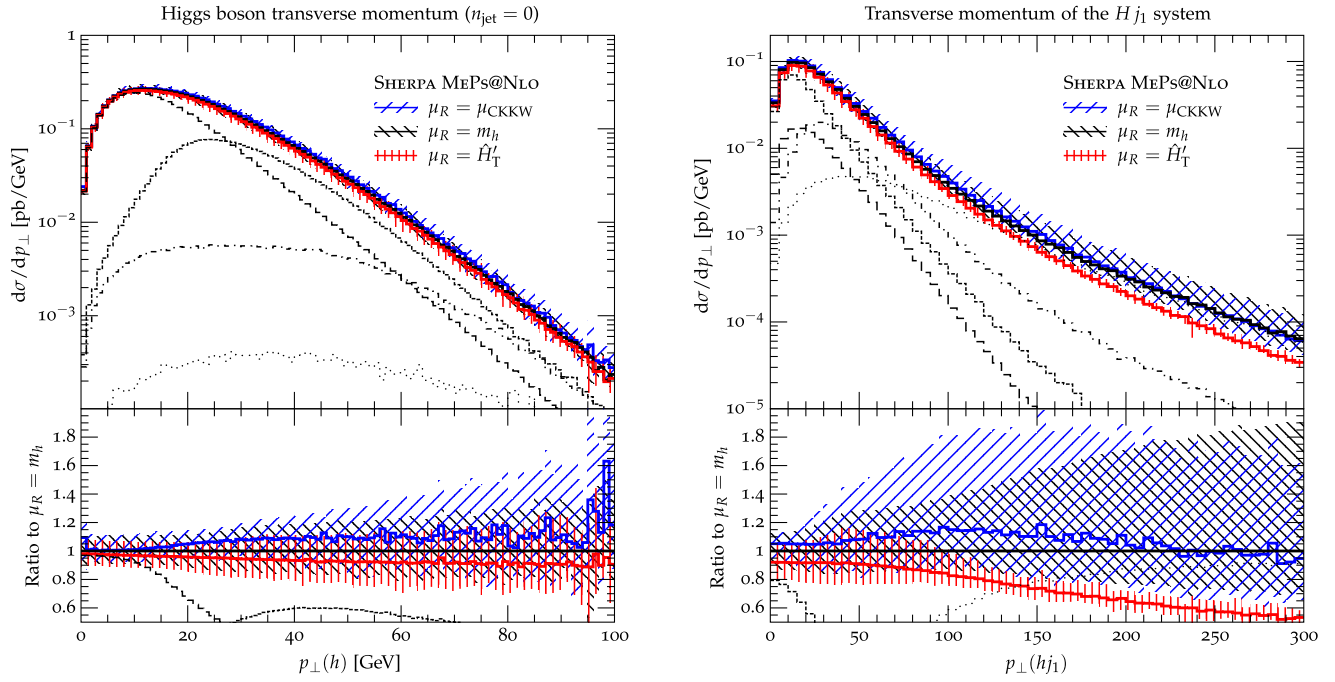


FIG. 2 (color online). Transverse momentum of the Higgs boson with a veto on jets of $p_T > 30$ GeV (left) and transverse momentum of the Higgs-jet system in presence of a jet with $p_T > 30$ GeV (right). For details see Fig. 1.

Figure 2 shows the Higgs transverse momentum distribution in the absence of any jet with transverse momentum larger than 30 GeV, and the transverse momentum distribution of the Higgs + jet system, $p_{T,hj}$, in the presence of a jet with $p_{T,j} > 30$ GeV. It is interesting to

observe that the uncertainties in $p_{T,hj}$ are of similar size at high transverse momentum for the CKKW scale and for $\mu_R = m_h$. This is because the CKKW scale in this case is driven by the lowest scale in the parton-shower tree, which is the scale of the core process, m_h . Correspondingly, the

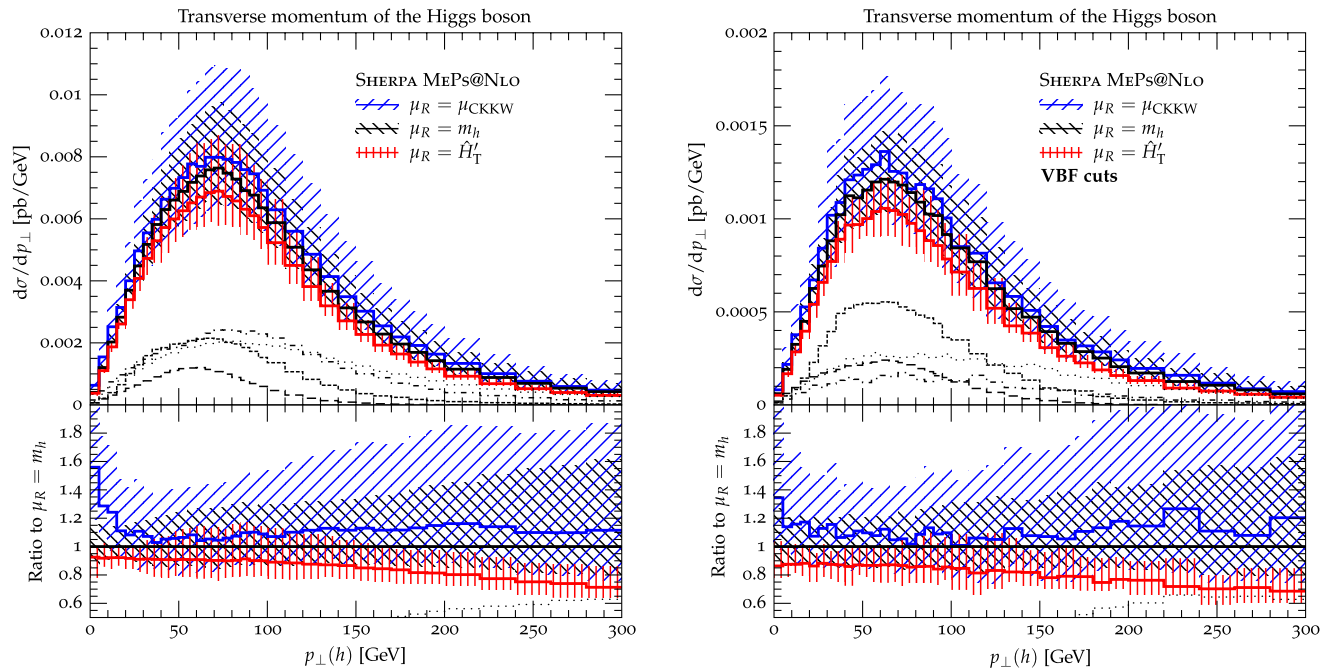


FIG. 3 (color online). Transverse momentum of the Higgs boson in the dijet (left) and VBF (right) selection with three different scale choices. For details see Fig. 1.

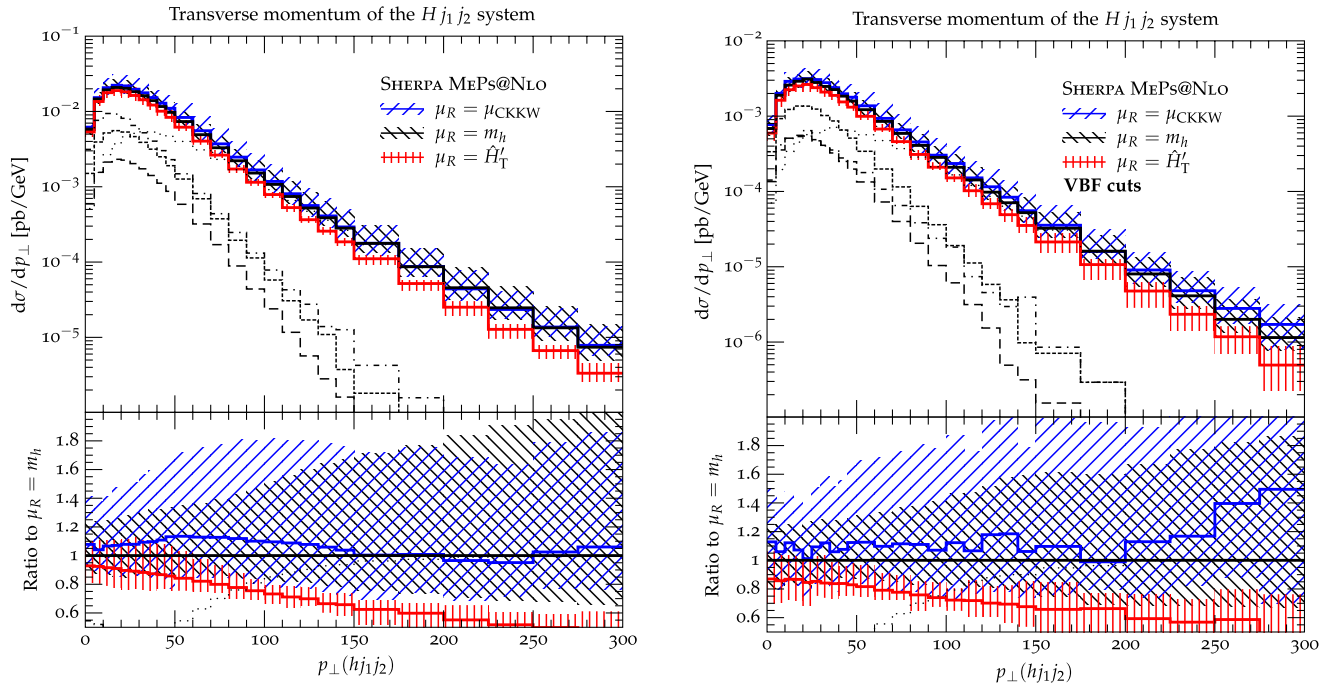


FIG. 4 (color online). Transverse momentum of the Higgs boson plus two leading jets system in the dijet (left) and VBF (right) selection with three different scale choices. For details see Fig. 1.

uncertainties of the Higgs boson p_T with a jet veto are of similar size for $\mu_R = m_h$ and for $\mu_R = \hat{H}'_T$, even at large transverse momenta. The difference in these scales is at most $\hat{H}'_T - m_h \lesssim 120$ GeV, as we include up to only three additional jets at fixed order in the simulation.

B. Dijet and VBF observables

Figure 3 shows the transverse momentum of the Higgs boson in the dijet and the VBF selection. In the VBF selection the cross section is considerably reduced, while the shape of the p_T spectrum stays largely the same. Note,

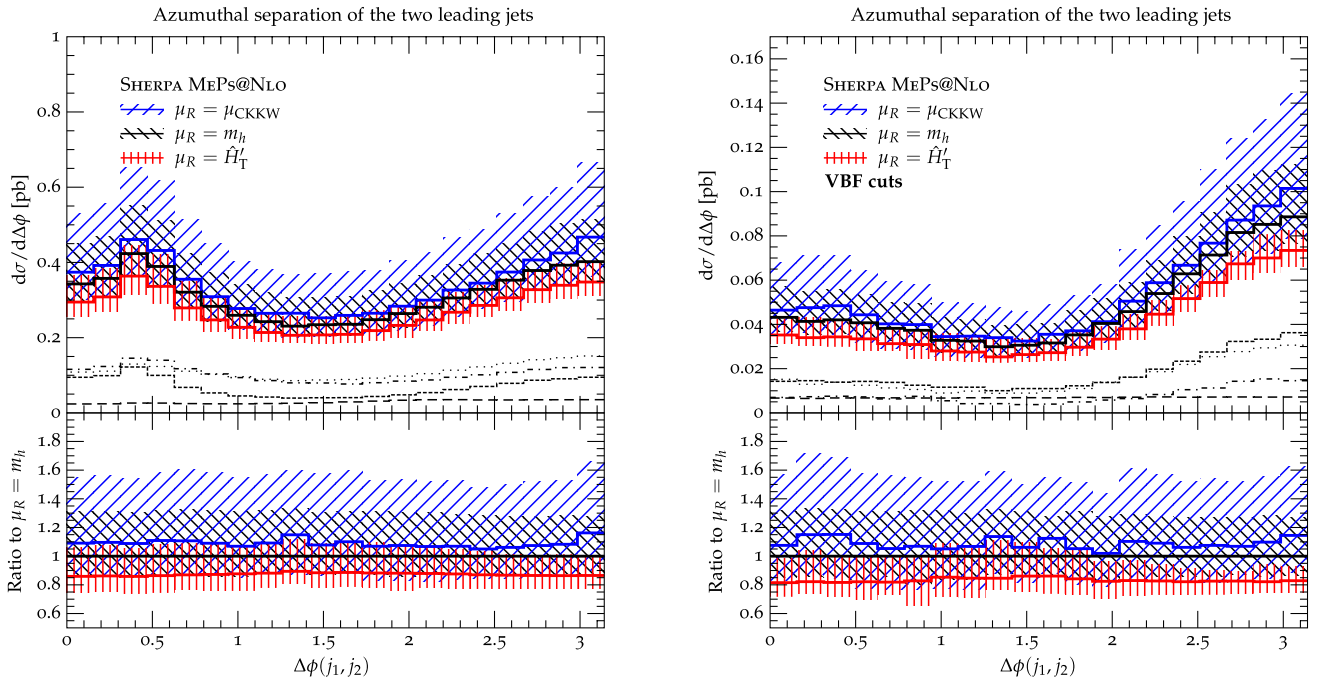


FIG. 5 (color online). Azimuthal separation of the two leading jets in the dijet (left) and VBF (right) selection with three different scale choices. For details see Fig. 1.

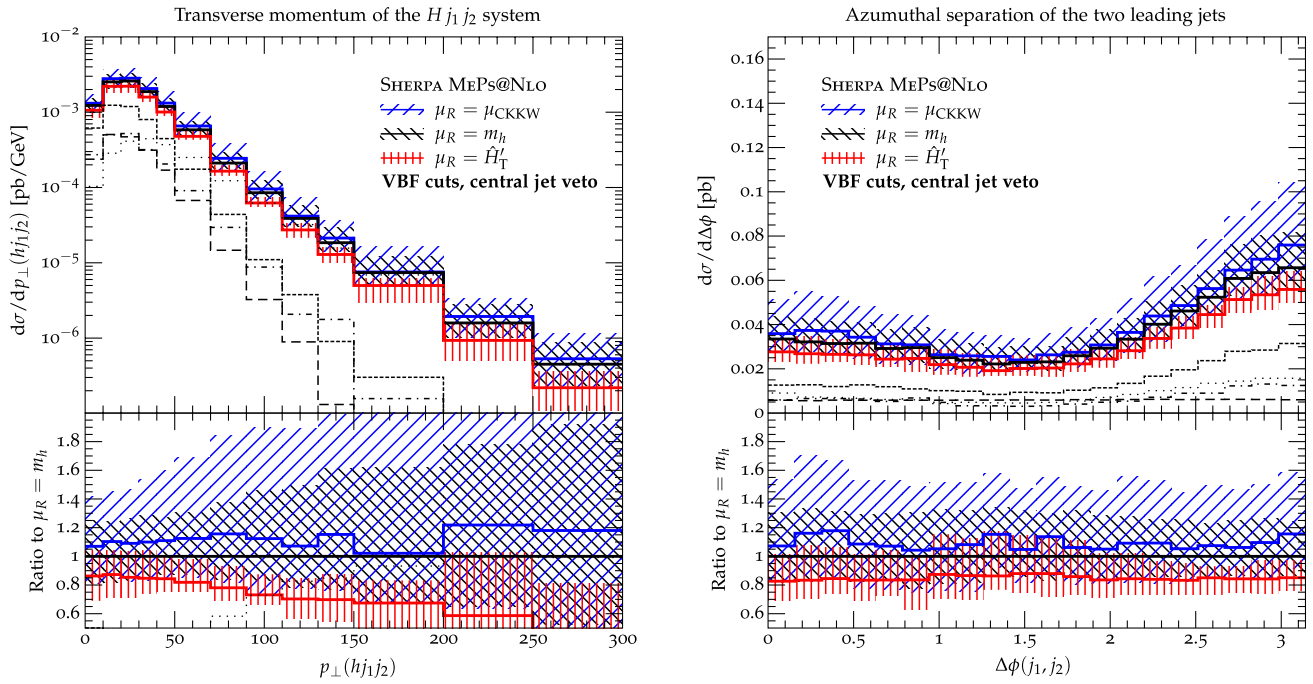


FIG. 6 (color online). Transverse momentum of the Higgs boson plus two leading jets system (left) and azimuthal separation of the two leading jets (right) with three different scale choices. For details see Fig. 1.

however, that the VBF selection increases the contribution from fixed-order events with exactly two hard jets, indicated by the dashed-dotted line in the figure. This confirms that also in the MEPS@NLO merged sample the VBF selection acts as an effective veto against a third jet, which

is—in gluon fusion processes—predominantly produced in the central region.

Figure 4 shows the combined transverse momentum of the Higgs boson and the two leading jets. It is apparent that the uncertainties for the CKKW scale and for $\mu_R = m_h$ are

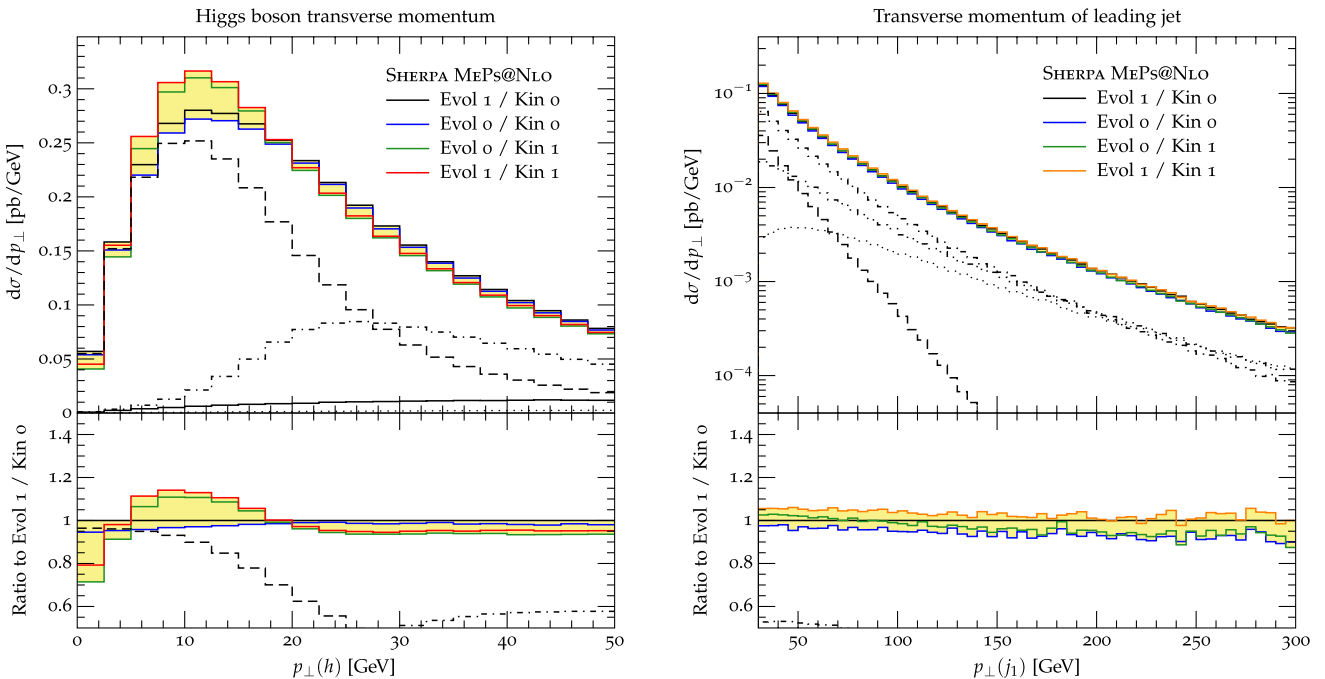


FIG. 7 (color online). Transverse momentum of the Higgs boson (left) and of the first jet (right) for different evolution variables and recoil schemes. See Sec. II for details and definition of the schemes.

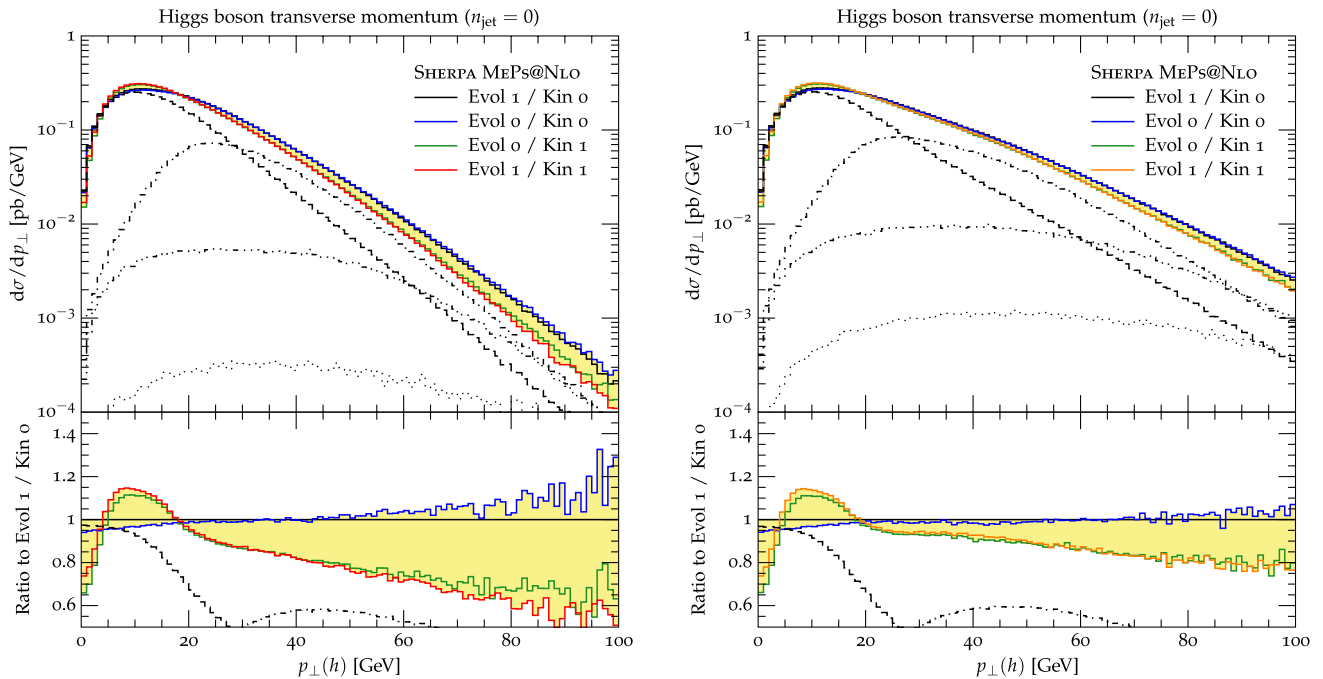


FIG. 8 (color online). Transverse momentum of the Higgs boson in absence of jets with $p_T > 30$ GeV (left) and $p_T > 50$ GeV (right) for different evolution variables and recoil schemes. See Sec. II for details and definitions of the schemes.

nearly identical in the high- p_T region, an effect which was also observed in Fig. 2. The low- p_T region shows a large spread between the different predictions, as they are driven in this case by their very different behavior with regard to adding an additional jet at small transverse momentum: In the CKKW scheme, the overall scale will be close to the transverse momentum of this jet, and therefore rather small. This leads to an increase in the cross section. For $\mu_R = \hat{H}_T^l$ the jet- p_T will increase the scale further, and the cross section will drop. The prediction for $\mu_R = m_h$ lies in between. Note that this distribution is effectively described at LO only.

Fig. 5 displays the azimuthal decorrelation between the Higgs boson and the dijet system, and the azimuthal decorrelation between the two leading jets, respectively. These observables do not exhibit a great sensitivity to the scale choice in the fixed-order calculation. The only variations come from a change in the total rate for Higgs plus dijet production, affecting normalization of the result and size of its uncertainty band, but not its functional form. It is interesting to note the effect of the VBF cuts on $\Delta\phi(j_1, j_2)$. In the plain dijet selection two maxima are apparent, one at the jet radius stemming from the two leading jets being produced collinearly, recoiling against the Higgs boson, and the other at $\Delta\phi = \pi$ stressing the importance dijetlike topologies with a rather soft Higgs produced centrally. While the latter configurations are enhanced by the VBF cuts, the former are suppressed.

With the introduction of a veto on jet production inbetween the two leading jets the shape of the

$\Delta\phi(j_1, j_2)$ distribution remains largely unaffected. Only its cross section is reduced, as can be seen in Fig. 6. The transverse momentum of the Higgs-plus-dijet system on the other hand is softened as its driving force, the production of a third jet, is constrained. Note again that this distribution is effectively described at LO only.

C. Parton shower uncertainties

In this subsection the intrinsic uncertainties of the parton shower are scrutinized. We compare the two evolution schemes in Table I and the two kinematics mappings described in Sec. II.

Figure 7 shows the transverse momentum of the Higgs boson and the transverse momentum of the leading jet. We expect the dominant effects of the kinematics mapping to be visible in the region which is most influenced by resummation. This is the low- p_T region in the case of the Higgs transverse momentum only. The transverse momentum distribution of the hardest jet should exhibit a smaller sensitivity to resummation, which is nicely exemplified by a very small uncertainty band.

Next we turn to the transverse momentum of the Higgs boson in absence of any jet of transverse momentum larger than 30 GeV (50 GeV), i.e. the transverse momentum of the Higgs boson in presence of a jet veto. This observable must naturally be extremely sensitive to the kinematics mapping in the high tail, because any transverse momentum is generated by subsequent emissions of comparably low transverse momentum. In other words, the large p_T of the Higgs boson in this case is built up by several mini-jets,

predominantly produced by soft gluon emission from initial-state partons. Figure 8 shows that the uncertainty arising from the kinematics mapping is indeed dominant in the high- p_T region, and that its size is considerably reduced when the cut on the jet- p_T is increased. This is expected, because with a higher jet- p_T cut the dominant radiation effects again are modeled by emission of a few semi-hard jets, rather than many soft gluons. This is also confirmed by the contributions from the various individual $pp \rightarrow h + n$ jet results shown in Fig. 8.

IV. CONCLUSIONS

We have presented an analysis of uncertainties in the merging of parton showers with NLO QCD calculations for Higgs-boson plus multi-jets through gluon fusion. We used the Monte Carlo event generator SHERPA for our study, in combination with virtual corrections obtained from MCFM.

The uncertainties arising from the perturbative QCD calculation are sizable, due to the α_s^2 -dependence of the lowest multiplicity leading-order process. This is reflected by the relatively large scale uncertainties, which are driven by the variation of the renormalization scale. The increased color charges in the initial state, compared to Drell-Yan processes, imply that resummation scale variations also have a much larger effect on the results. Additionally, the intrinsic parton-shower uncertainties, which we quantified through variations of the momentum mapping and the evolution parameter, have a large impact on observables involving a jet veto.

Consequently, the intrinsic uncertainties of the simulation are simultaneously driven by both the fixed-order part of the calculation and the resummation. In similar analyses of Drell-Yan lepton pair production, a large improvement was observed when performing the merging at NLO

accuracy [2]. Deficiencies of the parton shower approximation could to some extent be cured by the fixed-order corrections. In Higgs-boson production the effects seem not as pronounced. Our analysis implies in particular that more work is necessary to improve the resummation implemented by parton showers. In particular, the uncertainties related to the definition of the momentum mapping pose an interesting problem which probably can successfully be dealt with only by enhancing the accuracy of the shower approximation. This should be seen in the context of striving for higher accuracy in particle-level simulations through including higher-order fixed order corrections. In our opinion, the potential improvement from including next-to-next-to-leading-order corrections in a Monte Carlo simulation could be partially absorbed by the residual, large uncertainties from parton showers.

ACKNOWLEDGMENTS

S. H.'s work was supported by the U.S. Department of Energy under Contract No. DE-AC02-76SF00515 and in part by the U.S. National Science Foundation, Grant No. NSF-PHY-0705682 (The LHC Theory Initiative). M. S. acknowledges supported by the Research Executive Agency (REA) of the European Union under the Grant Agreements No. PITN-GA-2010-264564 (LHCPhenoNet) and No. PITN-GA-2012-315877 (MCnet). F. K. acknowledges support by the REA under Contract No. PITN-GA-2012-316704 (HiggsTools). M. S. would further like to acknowledge fruitful discussions on the subject within the ‘‘Jets in Higgs physics’’ working group for YR3 [54] and at Les Houches 2013. This research was performed using resources provided by the Open Science Grid, which is supported by the National Science Foundation and the U.S. Department of Energy’s Office of Science [55].

-
- [1] S. Höche, F. Krauss, M. Schönherr, and F. Siegert, *J. High Energy Phys.* **09** (2012) 049; *Phys. Rev. Lett.* **110**, 052001 (2013); *Phys. Rev. D* **86**, 094042 (2012).
 - [2] S. Höche, F. Krauss, M. Schönherr, and F. Siegert, *J. High Energy Phys.* **04** (2013) 027; T. Gehrmann, S. Höche, F. Krauss, M. Schönherr, and F. Siegert, *J. High Energy Phys.* **01** (2013) 144.
 - [3] S. Frixione and B. R. Webber, *J. High Energy Phys.* **06** (2002) 029; S. Frixione, F. Stoeckli, P. Torrielli, and B. R. Webber, *J. High Energy Phys.* **01** (2011) 053; S. Plätzer and S. Gieseke, *Eur. Phys. J. C* **72**, 2187 (2012).
 - [4] S. Schumann and F. Krauss, *J. High Energy Phys.* **03** (2008) 038.
 - [5] S. Catani and M. H. Seymour, *Nucl. Phys.* **B485**, 291 (1997).
 - [6] S. Höche, S. Schumann, and F. Siegert, *Phys. Rev. D* **81**, 034026 (2010); T. Carli, T. Gehrmann, and S. Höche, *Eur. Phys. J. C* **67**, 73 (2010).
 - [7] S. Plätzer and S. Gieseke, *J. High Energy Phys.* **01** (2011) 024.
 - [8] K. Hamilton and P. Nason, *J. High Energy Phys.* **06** (2010) 039.
 - [9] S. Höche, F. Krauss, M. Schönherr, and F. Siegert, *J. High Energy Phys.* **08** (2011) 123.
 - [10] L. Lönnblad and S. Prestel, *J. High Energy Phys.* **03** (2013) 166.
 - [11] R. Frederix and S. Frixione, *J. High Energy Phys.* **12** (2012) 061.
 - [12] K. Hamilton, P. Nason, and G. Zanderighi, *arXiv:1206.3572*.

- [13] K. Hamilton, P. Nason, C. Oleari, and G. Zanderighi, *J. High Energy Phys.* **05** (2013) 082.
- [14] P. Nason, *J. High Energy Phys.* **11** (2004) 040; S. Frixione, P. Nason, and C. Oleari, *J. High Energy Phys.* **11** (2007) 070; S. Alioli, P. Nason, C. Oleari, and E. Re, *J. High Energy Phys.* **04** (2009) 002; K. Hamilton, P. Richardson, and J. Tully, *J. High Energy Phys.* **04** (2009) 116; S. Höche, F. Krauss, M. Schönherr, and F. Siegert, *J. High Energy Phys.* **04** (2011) 024; J. M. Campbell, R. Ellis, R. Frederix, P. Nason, C. Oleari, and C. Williams, *J. High Energy Phys.* **07** (2012) 092.
- [15] S. Höche, F. Krauss, S. Schumann, and F. Siegert, *J. High Energy Phys.* **05** (2009) 053.
- [16] L. Lönnblad, *J. High Energy Phys.* **05** (2002) 046.
- [17] G. Aad *et al.* (ATLAS Collaboration), *Phys. Lett. B* **716**, 1 (2012); S. Chatrchyan *et al.* (CMS Collaboration), *Phys. Lett. B* **716**, 30 (2012).
- [18] F. Englert and R. Brout, *Phys. Rev. Lett.* **13**, 321 (1964); P. W. Higgs, *Phys. Rev. Lett.* **13**, 508 (1964); G. Guralnik, C. Hagen, and T. Kibble, *Phys. Rev. Lett.* **13**, 585 (1964); T. Kibble, *Phys. Rev.* **155**, 1554 (1967).
- [19] K. Melnikov and F. Petriello, *Phys. Rev. Lett.* **96**, 231803 (2006); M. Grazzini, *J. High Energy Phys.* **02** (2008) 043.
- [20] R. Boughezal, F. Caola, K. Melnikov, F. Petriello, and M. Schulze, *J. High Energy Phys.* **06** (2013) 072.
- [21] R. V. Harlander, T. Neumann, K. J. Ozeren, and M. Wiesemann, *J. High Energy Phys.* **08** (2012) 139.
- [22] C. Anastasiou, C. Duhr, F. Dulat, F. Herzog, and B. Mistlberger, *J. High Energy Phys.* **12** (2013) 088; W. B. Kilgore, [arXiv:1312.1296](https://arxiv.org/abs/1312.1296).
- [23] C. Anastasiou, C. Duhr, F. Dulat, E. Furlan, T. Gehrmann, F. Herzog, and B. Mistlberger, [arXiv:1403.4616](https://arxiv.org/abs/1403.4616); C. Anastasiou, R. Boughezal, and F. Petriello, *J. High Energy Phys.* **04** (2009) 003.
- [24] S. Actis, G. Passarino, C. Sturm, and S. Uccirati, *Phys. Lett. B* **670**, 12 (2008).
- [25] J. M. Campbell, R. K. Ellis, and G. Zanderighi, *J. High Energy Phys.* **100** (2006) 028; J. M. Campbell, R. K. Ellis, and C. Williams, *Phys. Rev. D* **81**, 074023 (2010); H. van Deurzen, N. Greiner, G. Luisoni, P. Mastrolia, E. Mirabella, G. Ossola, T. Peraro, J. F. von Soden-Fraunhofen, and F. Tramontano, *Phys. Lett. B* **721**, 74 (2013).
- [26] G. Cullen, H. van Deurzen, N. Greiner, G. Luisoni, P. Mastrolia, E. Mirabella, G. Ossola, T. Peraro, and F. Tramontano, *Phys. Rev. Lett.* **111**, 131801 (2013).
- [27] D. de Florian and M. Grazzini, *Phys. Lett. B* **674**, 291 (2009); D. de Florian, G. Ferrera, M. Grazzini, and D. Tommasini, *J. High Energy Phys.* **06** (2012) 132.
- [28] A. Banfi, G. P. Salam, and G. Zanderighi, *J. High Energy Phys.* **06** (2012) 159; A. Banfi, P. F. Monni, G. P. Salam, and G. Zanderighi, *Phys. Rev. Lett.* **109**, 202001 (2012); F. J. Tackmann, J. R. Walsh, and S. Zuberi, *Phys. Rev. D* **86**, 053011 (2012); I. W. Stewart, F. J. Tackmann, J. R. Walsh, and S. Zuberi, [arXiv:1307.1808](https://arxiv.org/abs/1307.1808); T. Becher and M. Neubert, *J. High Energy Phys.* **07** (2012) 108; T. Becher, M. Neubert, and D. Wilhelm, *J. High Energy Phys.* **05** (2013) 110; T. Becher, M. Neubert, and L. Rothen, *J. High Energy Phys.* **10** (2013) 125; X. Liu and F. Petriello, *Phys. Rev. D* **87**, 094027 (2013).
- [29] K. Hamilton, P. Nason, E. Re, and G. Zanderighi, *J. High Energy Phys.* **10** (2013) 222.
- [30] S. Plätzer and M. Sjö Dahl, *J. High Energy Phys.* **07** (2012) 042.
- [31] S. Catani, F. Krauss, R. Kuhn, and B. R. Webber, *J. High Energy Phys.* **11** (2001) 063; F. Krauss, *J. High Energy Phys.* **08** (2002) 015.
- [32] K. Hamilton, P. Richardson, and J. Tully, *J. High Energy Phys.* **11** (2009) 038.
- [33] F. Cascioli, S. Höche, F. Krauss, P. Maierhöfer, S. Pozzorini, and F. Siegert, *J. High Energy Phys.* **01** (2014) 046.
- [34] S. Höche, J. Huang, G. Luisoni, M. Schönherr, and J. Winter, *Phys. Rev. D* **88**, 014040 (2013).
- [35] S. Plätzer, *J. High Energy Phys.* **08** (2013) 114.
- [36] M. L. Mangano, M. Moretti, F. Piccinini, and M. Treccani, *J. High Energy Phys.* **01** (2007) 013; J. Alwall *et al.*, *Eur. Phys. J. C* **53**, 473 (2008).
- [37] D. L. Rainwater and D. Zeppenfeld, *J. High Energy Phys.* **12** (1997) 005; D. L. Rainwater, D. Zeppenfeld, and K. Hagiwara, *Phys. Rev. D* **59**, 014037 (1998); T. Plehn, D. L. Rainwater, and D. Zeppenfeld, *Phys. Rev. D* **61**, 093005 (2000).
- [38] Y. L. Dokshitzer, S. Troian, and V. A. Khoze, *Sov. J. Nucl. Phys.* **46**, 712 (1987); Y. L. Dokshitzer, V. A. Khoze, and T. Sjöstrand, *Phys. Lett. B* **274**, 116 (1992).
- [39] T. Han, G. Valencia, and S. Willenbrock, *Phys. Rev. Lett.* **69**, 3274 (1992); M. Spira, *Fortschr. Phys.* **46**, 203 (1998); T. Figy, C. Oleari, and D. Zeppenfeld, *Phys. Rev. D* **68**, 073005 (2003); T. Figy and D. Zeppenfeld, *Phys. Lett. B* **591**, 297 (2004); E. L. Berger and J. M. Campbell, *Phys. Rev. D* **70**, 073011 (2004).
- [40] P. Bolzoni, F. Maltoni, S.-O. Moch, and M. Zaro, *Phys. Rev. Lett.* **105**, 011801 (2010); *Phys. Rev. D* **85**, 035002 (2012).
- [41] T. Figy, V. Hankele, and D. Zeppenfeld, *J. High Energy Phys.* **02** (2008) 076; F. Campanario, T. Figy, S. Plätzer, and M. Sjö Dahl, *Phys. Rev. Lett.* **111**, 211802 (2013).
- [42] M. Ciccolini, A. Denner, and S. Dittmaier, *Phys. Rev. D* **77**, 013002 (2008).
- [43] P. Nason and C. Oleari, *J. High Energy Phys.* **02** (2010) 037; L. D'Errico and P. Richardson, [arXiv:1106.3939](https://arxiv.org/abs/1106.3939); S. Frixione, P. Torrielli, and M. Zaro, *Phys. Lett. B* **726**, 273 (2013).
- [44] T. Gleisberg, S. Höche, F. Krauss, A. Schälicke, S. Schumann, and J. Winter, *J. High Energy Phys.* **02** (2004) 056; T. Gleisberg, S. Höche, F. Krauss, M. Schönherr, S. Schumann, F. Siegert, and J. Winter, *J. High Energy Phys.* **02** (2009) 007.
- [45] J. M. Campbell and R. Ellis, *Nucl. Phys. B, Proc. Suppl.* **205–206**, 10 (2010); J. Campbell, R. K. Ellis, and C. Williams, <http://mcfm.fnal.gov>.
- [46] J. R. Ellis, M. K. Gaillard, and D. V. Nanopoulos, *Nucl. Phys. B* **106**, 292 (1976); F. Wilczek, *Phys. Rev. Lett.* **39**, 1304 (1977); M. A. Shifman, A. Vainshtein, M. Voloshin, and V. I. Zakharov, *Sov. J. Nucl. Phys.* **30**, 711 (1979); J. R. Ellis, M. Gaillard, D. V. Nanopoulos, and C. T. Sachrajda, *Phys. Lett.* **83B**, 339 (1979).

- [47] F. Krauss, R. Kuhn, and G. Soff, *J. High Energy Phys.* **02** (2002) 044; T. Gleisberg and F. Krauss, *Eur. Phys. J. C* **53**, 501 (2008).
- [48] S. Dawson, *Nucl. Phys.* **B359**, 283 (1991); A. Djouadi, M. Spira, and P. Zerwas, *Phys. Lett. B* **264**, 440 (1991).
- [49] D. de Florian, M. Grazzini, and Z. Kunszt, *Phys. Rev. Lett.* **82**, 5209 (1999); V. Ravindran, J. Smith, and W. Van Neerven, *Nucl. Phys.* **B634**, 247 (2002).
- [50] H.-L. Lai, M. Guzzi, J. Huston, Z. Li, P. M. Nadolsky, J. Pumplin, and C.-P. Yuan, *Phys. Rev. D* **82**, 074024 (2010); J. Gao, M. Guzzi, J. Huston, H.-L. Lai, Z. Li, P. Nadolsky, J. Pumplin, D. Stump, C.-P. Yuan, [arXiv:1302.6246](https://arxiv.org/abs/1302.6246).
- [51] M. Cacciari, G. P. Salam, and G. Soyez, *J. High Energy Phys.* **04** (2008) 063.
- [52] C. F. Berger, Z. Bern, L. J. Dixon, F. Febres-Cordero, D. Forde, T. Gleisberg, H. Ita, D. A. Kosower, and D. Maître, *Phys. Rev. Lett.* **106**, 092001 (2011).
- [53] A. Buckley, J. Butterworth, L. Lönnblad, D. Grellscheid, H. Hoeth, L. Lönnblad, J. Monk, H. Schulz, and F. Siegert, *Comput. Phys. Commun.* **184**, 2803 (2013).
- [54] S. Heinemeyer *et al.* (LHC Higgs Cross Section Working Group), Report No. 10.5170/CERN-2013-004.
- [55] R. Pordes, M. Altunay, P. Avery, A. Bejan, K. Blackburn, A. Blatecky, R. Gardner, B. Kramer, M. Livny, J. McGee *et al.* (Open Science Grid), *J. Phys. Conf. Ser.* **125**, 012070 (2008); L. Bauerdick, M. Ernst, D. Fraser, M. Livny, R. Pordes, C. Sehgal, and F. Würthwein (Open Science Grid), *J. Phys. Conf. Ser.* **396**, 042048 (2012).